Final Report for the FY-2017 FES Theory and Simulation Performance Target

J.-P. Lee[(a)], D. B. Batchelor[(b)], W. Elwasif[(c)], S. Frank[(a)], J. C. Wright[(a)], and P. T. Bonoli[(a)]

[(a)]Plasma Science and Fusion Center, Massachusetts Institute of Technology, Cambridge, MA
[(b)]DIDITCO, Knoxville, TN
[(c)]Oak Ridge National Laboratory, Oak Ridge, TN

The FY-2017 FES Theory and Simulation Performance Target

"Lower hybrid current drive (LHCD) will be indispensable for driving off-axis current during long-pulse operation of future burning plasma experiments including ITER, since it offers important leverage for controlling damaging transients caused by magnetohydrodynamic instabilities. However, the experimentally demonstrated high efficiency of LHCD is incompletely understood. In FY 2017, massively parallel, high-resolution simulations with 480 radial elements and 4095 poloidal modes will be performed using full-wave radiofrequency field solvers and particle Fokker-Planck codes to elucidate the roles of toroidicity and full-wave effects. The simulation predictions will be compared with experimental data from the superconducting EAST tokamak."

Executive Summary

As stated in the language of the FY-2017 FES Theory and Simulation Performance Target, lower hybrid current drive (LHCD) will be indispensable for driving off-axis current during long-pulse operation of future burning plasma experiments including ITER. However, the experimentally demonstrated high efficiency of LHCD is not completely understood because LH waves used in these experiments are typically injected at values of the parallel (along **B**) phase speed $v_{//}$ that are much greater than the phase speed where linear electron Landau is strongest; namely at $v_{//} \sim (2.5\text{-}3)\times v_{te}$, where $v_{te} = (2T_e/m_e)^{1/2}$. Thus, these wave are expected to be only weakly damped. This turns out to be the case when the background electron temperature is of order $T_e \sim 3$ keV and the parallel refractive index of the LH waves is $n_{//} = c/v_{//} \sim 2$, which is typical of LHCD experiments in the EAST Tokamak.

A number of physical mechanisms have been proposed that would modify the injected LH waveguide spectrum causing the parallel phase speed to decrease to $\sim 3\times v_{te}$. These include toroidally induced changes in the parallel wavenumber due to the nonconstancy of the poloidal mode number in toroidal geometry, scattering of LH waves from density fluctuations in the plasma scrape-off layer, and broadening of the incident wave spectrum due to nonlinear parametric decay instability [Bonoli 2014]. In this Theory and Simulation Performance Target we utilize the TorLH electromagnetic field solver [Wright 2009] combined with the 3D (r, $v_\perp$, $v_{//}$) bounce averaged Fokker Planck code CQL3D [Harvey 1992] to assess the importance of full-wave effects on the deposition of LH waves in the EAST device. Prior simulations comparing hard x-ray spectra predicted by a combined ray tracing / Fokker Planck model (GENRAY / CQL3D) and a full-wave / Fokker Planck model (TorLH / CQL3D) found important differences in the shape and magnitude of the simulated spectra with the spectra simulated from the full-wave / Fokker Planck model in better agreement with measurements from the Alcator C-Mod

tokamak [Wright 2014]. These finding calls into question the validity of the ray tracing approach in a device such as EAST device where LH waves are not absorbed on the first pass into the plasma core. In this case, it is important to assess the importance of full-wave effects at locations such as plasma cut-offs where the waves reflect after incomplete absorption in the core. Furthermore, diffractional broadening of the LH wave front can occur at caustic surfaces where the geometrical optics description also breaks down. Finally, the quasilinear diffusion coefficient, which connects the full-wave and Fokker Planck solvers, is formulated more accurately from full-wave fields than in ray tracing treatments.

There were significant algorithmic and computer science challenges that had to be overcome in order to accomplish the 2017 FES Theory and Simulation Performance Target. As discussed in the First Quarter Milestone section, the electric field in TorLH is expressed as a sum over poloidal modes [see Eq. (1)] and in order to resolve the shortest wavelength in the system it was necessary to use $N_m = 4095$ modes. This turns out to be the largest simulation that has ever been performed with the field solver, utilizing (32,000-33,000) cores for (0.66-1.0) wall clock hours on the Edison platform (each time the field solver is executed). The TorLH-CQL3D iteration consists of a complex multi-step workflow that was automated under the Integrated Plasma Simulator (IPS) framework [Batchelor 2009]. It was necessary to make significant modifications to the IPS in order to handle this workflow which consists of (i) running the TorLH full-wave solver to obtain the LHRF electric fields using the most recent iterate for the nonthermail electron distribution function; (ii) reconstructing the quasilinear RF diffusion coefficient from the LHRF wave fields computed in Step (i); (iii) running the CQL3D Fokker Planck solver to advance the electron distribution function in time using the quasilinear RF diffusion coefficient computed in Step (ii); and (iv) creating a table of interpolating values for $Im\{\chi_{zz}\} \propto \partial f_e / \partial p_{//}$ using the electron distribution function computed by CQLD in Step (iii). Here f_e is the electron distribution function, $p_{//}$ is the parallel relativistic momentum, and χ_{zz} corresponds to the Stix dielectric tensor element and gives the electron Landau damping physics. It was also necessary to reformulate the quasilinear diffusion coefficient in a form that guarantees positive definite power deposition [Lee 2018]. In order to maintain self-consistency between the local wave damping and the quasilinear diffusion coefficient, the LH power was turned on gradually [see Eq. (3)], thus allowing use of the explicit fixed-point iteration scheme described by the workflow in Steps (i) – (iv) above.

The following critical computational and physics goals were accomplished as part of this Theory and Simulation Performance Target:

- Demonstrated the convergence properties of the TorLH full-wave solver for parameters characteristic of EAST LHCD experiments using $T_e(0) = 3.2$ keV and $n_{//} = -1.8$ with 4095 poloidal modes and using $T_e(0) = 9.5$ keV and n// = -1.8 with 2047 poloidal modes. In each of these cases, the plasma was discretized into 480 elements in the radial direction.
- Demonstrated numerical convergence between the full-wave and Fokker Planck solvers at moderate poloidal mode resolution (1023 poloidal modes) using a scheme whereby the LH power was turned on slowly over 10 iterations in order to maintain self-consistency between the RF quasilinear diffusion coefficient and the nonthermal electron distribution function. The converged quasilinear power deposition profiles were found to be peaked off-axis in qualitative agreement with the predictions of ray tracing / Fokker Planck simulations [Shiraiwa 2015]. Because the poloidal mode resolution was limited to 1023

modes in these simulations, the LH wave fields computed by the field solver were not fully converged.

- Carried out an iterated simulation with TorLH and CQL3D using 4095 modes in the field solver to obtain completely converged electric wave solutions. Although the simulation had to be terminated at five iterations because of hardware failure issues on Edison, the LHRF power deposition profiles although not yet converged, were found to be peaked off-axis, in qualitative agreement with ray tracing / Fokker Planck predictions.

The preliminary conclusion from execution of this Theory and Simulation Performance Target is that full-wave / Fokker Planck and ray tracing / Fokker Planck simulations are in qualitative agreement with each other, with both predicting off-axis LHRF power deposition profiles. Significantly, these predictions disagree with the experimental measurements of hard x-ray emission in these experiments, which support the conclusion that some fraction of the LHRF power is being deposited on-axis [Shiraiwa 2015]. In ongoing work, we are now extending the iterated simulations with TorLH and CQL3D using 4095 poloidal modes out to 10-15 iterations in order to fully converge the quasilinear power deposition profiles. In the remainder of this report we describe in detail the quarterly milestones and progress that constituted this Theory and Simulation Performance Target.

1. Completion of the First Quarter Milestone

Carry out a poloidal mode scan with the TorLH electromagnetic field solver using Maxwellian electrons and EAST discharge parameters, using 480 radial elements and 511, 1023, 2047, and 4095 poloidal modes. Confirm convergence of the LH electric field solution on all flux surfaces and the accuracy of the absorption and Poynting flux calculations for a case at high electron temperature. Repeat this poloidal mode scan at lower electron temperatures typical of actual EAST experiments where the LH waves undergo many reflections at the plasma edge before being absorbed collisionlessly via electron Landau damping.

1(a) Summary

The most challenging part of the first quarter milestone was to perform a poloidal mode scan using the TorLH electromagnetic field solver in order to confirm numerical convergence of the lower hybrid (LH) electric field solution on all flux surfaces in the EAST tokamak, at parameters typical of actual EAST LH current drive (LHCD) experiments. In these simulations the electron temperature is Maxwellian and low [$T_e(0) = 3.2$ keV], relative to the electron temperature needed to guarantee single pass absorption of the LH wave front [$T_e(0) \approx$ 9-10 keV]. The parallel refractive index ($n_{//} = c / v_{//}$) of the LH waves coupled in EAST is $n_{//} = -1.8$ and the electron temperature needed for these waves to be absorbed via linear electron Landau damping (ELD) is given by the condition $T_e(\text{keV}) \approx 30 / (n_{//})^2$. Thus the damping is weak at $T_e \sim 3$ keV for $n_{//} = -1.8$. Other parameters used in these simulations were $B_0 = 2.31$ T, $I_p = 373$ kA, a = 0.42 m, $R_0 = 1.85$ m, and $n_e(0) = 3.6 \times 10^{19}$ m^{-3}. The number of poloidal modes (N_m) used in the spectral representation of the electric field in TorLH [see Eq. (1)] was scanned through values of N_m = 511, 1023, 2047, and 4095 using a fixed number of radial elements (480). The 4095 mode requirement to converge numerical solutions on all flux surfaces is close to analytic estimates, where the fundamental criterion is that enough poloidal modes (m) must be retained in order to resolve the shortest perpendicular wavelength in the system, where $-N_m/2 < m < +N_m/2$ and $(N_m/2) \approx r \times k_\perp$. Here r is the minor radial position in the tokamak and $k_\perp$ is the perpendicular (to **B**) wavenumber of the LH wave. The 4095 mode simulation was performed at NERSC using 32,256 cores and required approximately one hour of wall clock time. The poloidal mode scan at higher electron temperature was not completed during the first quarter because of extra time that was needed for implementation of the TorLH field solver on the Edison platform. However, it was expected that complete numerical convergence of the field solution would be obtained at even lower values of N_m when using higher electron temperature because of the stronger linear Landau damping that occurs as T_e increases.

1(b) Details of First Quarter Progress

The electric field in the TorLH solver is expressed via a spectral Ansatz that is a sum over poloidal and toroidal modes as given by Eq. (1):

$$\vec{E}(\vec{x}) = \sum_{m,n_\phi} \vec{E}_{m,n}(\psi) e^{im\theta + in\phi} \qquad (1)$$

Thus a good test of numerical convergence is to plot the magnitude of the Fast Fourier Transform (FFT) of an electric field component (in this case the Re{E_ζ}) versus poloidal mode number (m) on each flux surface in order to determine if enough terms have been retained in the sum. Here E_ζ is the toroidal component of the electric field. The numerical convergence results for the EAST case in terms of this criterion are shown in Figs (1a) – 1(d) for N_m = 511, 1023, 2047, and 4095 modes. The different color curves correspond to different flux surfaces with tan, red, blue, green, gray, and black corresponding respectively to r/a = (0.1, 0.3, 0.5, 0.7, 0.9, 1.0). It can be clearly seen that as the number of poloidal modes increases there is a uniform progression of converged flux surfaces starting in the core (r/a = 0.1- 0.3) and finally out to the edge which is consistent with the analytic condition quoted earlier for numerical convergence whereby $(N_m/2) \approx r \times k_\perp$.

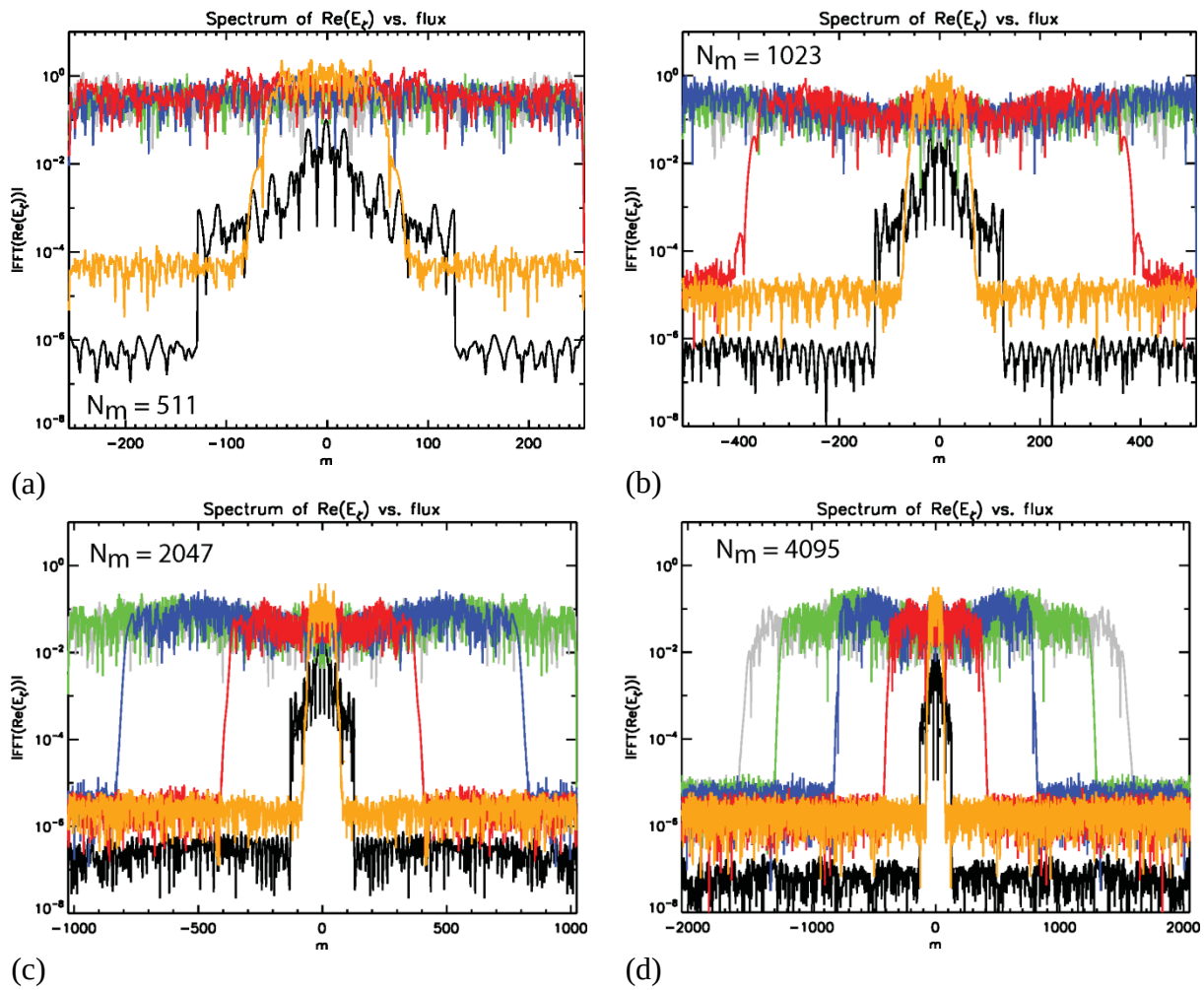

Figure 1: |FFT {Re(E_ζ)}| versus m from the TorLH solver for (a) N_m = 511, (b) N_m = 1023, (c) N_m = 2047, and (d) N_m = 4095. The tan, red, blue, green, gray, and black traces correspond respectively to r/a = (0.1, 0.3, 0.5, 0.7, 0.9, 1.0). The waveguide source is located at r/a = 1.0.

Figures 2(a) and 2(b) show how the spatial profile of ELD changes dramatically as N_m increases from 511 to 4095 and the electric field solution converges. Broadening of the LHRF power deposition profile as N_m increases is consistent with adding higher $k_{//}$ components to the spectral solution in TorLH that correspond to higher poloidal mode number (m) and thus damp at larger radii. The electric field solutions shown in Figs. 2(c) and 2(d) are consistent with the change in power absorption that is seen as N_m increases with the electric field intensity peaked in the core at 511 modes and moving off-axis and to the high field side at 4095 modes. The appearance of higher electric field intensity on the high field side in Fig. 2(d) is probably due to the fact that LH wave accessibility and wave penetration is better on the high field side owing to the higher toroidal magnetic field at that location. Interestingly the numerically converged power absorption in Fig. 2(b) has been found to be qualitatively similar to what is predicted by toroidal ray tracing analysis when a Maxwellian electron distribution function is also used.

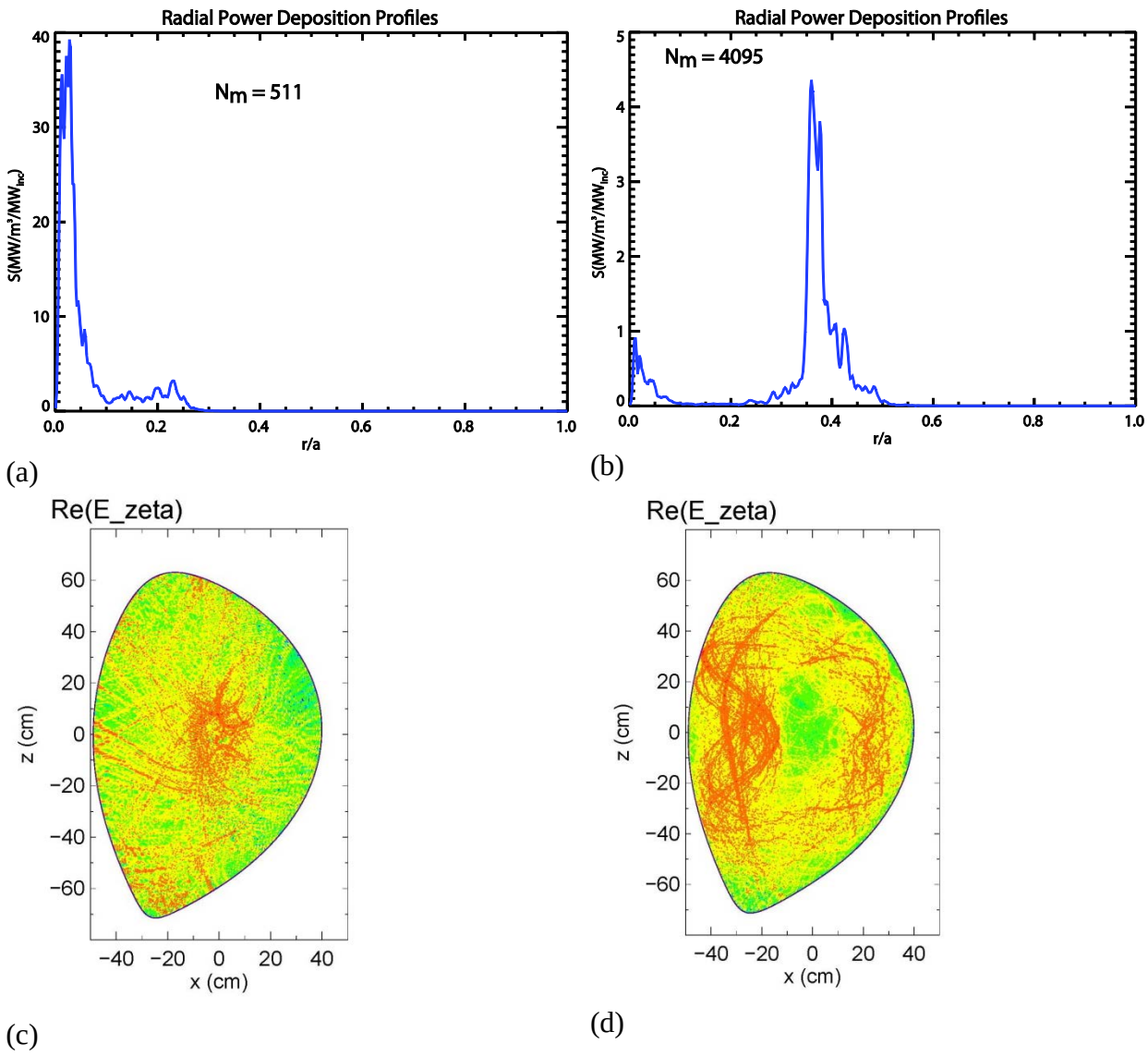

Figure 2: LHRF power deposition profiles from TorLH simulation at (a) $N_m = 511$ and (b) $N_m = 4095$ (b). Corresponding LH electric field contours for (c) $N_m = 511$ and (d) $N_m = 4095$.

2. Completion of the Second Quarter Milestone

Complete a reformulation of the quasilinear RF diffusion coefficient that guarantees positive definiteness in the lower hybrid range of frequencies (LHRF). Verify numerical implementation of the new formulation at high poloidal mode number (1023, 2047, and 4095 modes) using Maxwellian electrons. Verification will be done by comparing the absorbed power density profile from the new diffusion coefficient formulation with the power deposition from ***J·E*** *simulated with TorLH.*

2(a) Summary

During the second quarter, we successfully completed an unfinished task from the first quarter milestone. Namely, we performed a poloidal mode scan with the TorLH electromagnetic field solver using Maxwellian electrons and EAST discharge parameters, using 480 radial elements and 511, 1023, and 2047 poloidal modes, which demonstrated convergence of the LH electric field solution on all flux surfaces for a case at high electron temperature [$T_e(0) = 9.5$ keV]. As expected because of the higher electron temperature it was not necessary to use 4095 poloidal modes in order to achieve convergence on all flux surfaces. This point will be discussed in more detail in the next section.

During this period we also completed implementation of the quasilinear RF diffusion coefficient of Kennel and Engelmann [Kennel & Engelmann 1966] in the TorLH solver in a form that guarantees positive definiteness in the LHRF regime. Dr. Jungpyo Lee led this work. It should be noted that the derived positive definite form is general and was first done for ion cyclotron range of frequency (ICRF) waves in a paper published by Dr. Lee in Plasma Physics and Controlled Fusion [Lee 2018]. Dr. Lee also presented these results at the 2017 Sherwood Theory Conference in Annapolis, Maryland in a paper titled "Modification of the quasilinear diffusion coefficients for ICRF wave plasmas in a toroidal geometry".

An outstanding task that still remained to be completed from the second quarter milestone was to verify numerical implementation of the new quasilinear diffusion coefficient formulation at high poloidal mode number (1023, 2047, and 4095 modes) using Maxwellian electrons. This was not completed in large part because of the time that was devoted to preparing a publication on the positive definite form of the RF diffusion coefficient.

2(b) Details of Second Quarter Progress

Recall that the electric field in the TorLH solver is expressed via a spectral Ansatz that is a sum over poloidal and toroidal modes as given by Eq. (1). During the second quarter, we demonstrated convergence of this spectral expansion on all flux surfaces in the EAST tokamak at an electron temperature that was high enough to guarantee single pass absorption of the LH wave front. Recall the parallel refractive index ($n_{//} = c / v_{//}$) of the LH waves coupled in EAST is $n_{//} = -1.8$ and the electron temperature needed for these waves to be absorbed via linear electron Landau damping (ELD) is given by the condition $T_e(\text{keV}) \approx 30 / (n_{//})^2$. In order to achieve

complete absorption of the wave in the core it is therefore necessary to take $T_e(0) \sim 9.5$ keV. Other parameters used in these simulations were $B_0 = 2.31$ T, $I_p = 373$ kA, a = 0.42 m, $R_0 = 1.85$ m, and $n_e(0) = 3.6 \times 10^{19}$ m^{-3}. The number of poloidal modes (N_m) used in the spectral representation of the electric field in TorLH [see Eq. (1)] was scanned through values of N_m = 511, 1023, and 2047 using a fixed number of radial elements (480). In this scan it was found that the electric field solution was converged on all flux surfaces for 2047 modes in contrast to the 4095 poloidal modes that was required at the lower central electron temperature of $T_e(0) = 3.2$ keV [compare Figs. 3(a) and 3(b)].

The observed scaling of the poloidal mode requirement for numerical convergence with electron temperature can be understood as follows. As explained earlier, achieving converged numerical solutions for the wave electric field on all flux surfaces requires that enough poloidal modes (m) be retained in order to resolve the shortest perpendicular wavelength in the system where $k_\perp = (2\pi / \lambda_\perp) \approx (m / r)$. The value of $k_\perp$ is set approximately through the electrostatic LH dispersion relation that can be written as:

$$k_\perp \approx \frac{m}{r} \approx \frac{\omega_{pe}}{\omega} k_\parallel, \qquad (2)$$

where ω_{pe} is the electron plasma frequency, $(\omega/2\pi)$ is LH source frequency, and $k_{//} = n_{//} (\omega/c)$. We take the value of $n_{//}$ to be set by the condition for strong electron Landau damping which was given above. Thus we would expect that if T_e is increased from 3.2 keV to 9.5 keV which is about a factor 3, then the $n_{//}$ (and hence the $k_\perp$through Eq. 2) needed for strong electron damping would decrease by roughly a factor of 1.72. The corresponding value of m that would needed to resolve that $k_\perp$ (see Eq. 2) would also be expected to decrease by a similar factor implying a reduction in N_m from 4095 to (4095 / 1.72) ~ 2380. This is qualitatively similar to the value of $N_m \sim 2047$ found in the mode scan for complete convergence.

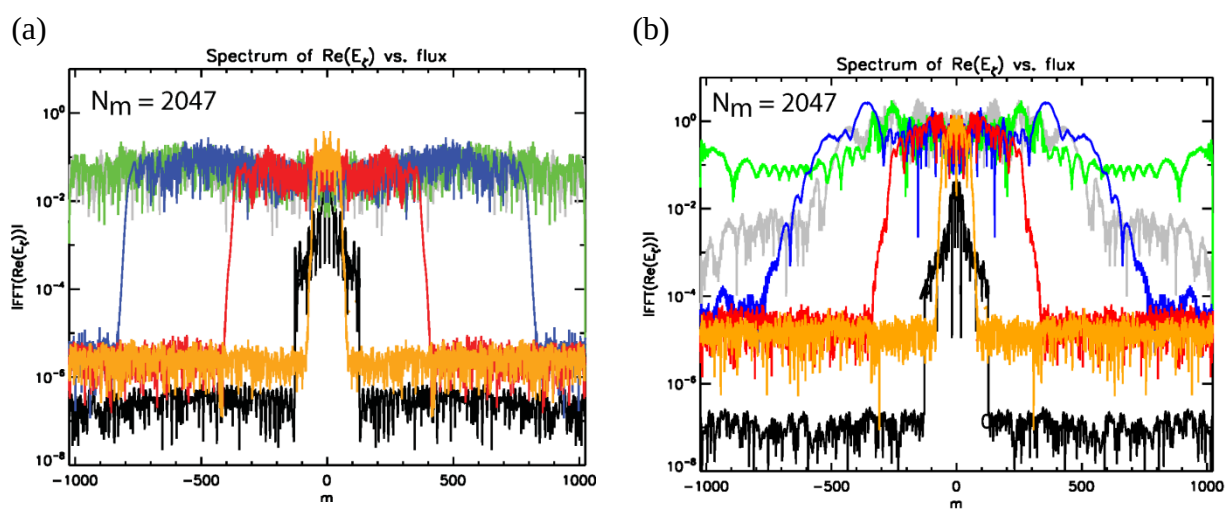

Figure 3: |FFT {Re(E_ζ)}| versus m from the TorLH solver for (a) $N_m = 2047$ and $T_e(0) = 3.2$ keV, and (b) $N_m = 2047$and $T_e(0) = 9.5$ keV. The tan, red, blue, green, gray, and black traces correspond respectively to r/a = (0.1, 0.3, 0.5, 0.7, 0.9, 1.0). The waveguide source is located at r/a = 1.0.

As discussed in the first quarter progress report a useful method for testing numerical convergence is to plot the magnitude of the Fast Fourier Transform (FFT) of an electric field component (in this case the Re{E_ζ}) versus poloidal mode number (m) on each flux surface in order to determine if enough modes have been retained in the sum. Here E_ζ is the toroidal component of the electric field. A comparison of the |FFT {Re(E_ζ)}| versus m for 2047 modes is shown in Fig. 3 for the lower temperature case [Fig. 3(a)] and the higher temperature case [Fig. 3(b)]. The different color curves correspond to different flux surfaces with tan, red, blue, green, gray, and black corresponding respectively to r/a = (0.1, 0.3, 0.5, 0.7, 0.9, 1.0). It can be seen that all flux surfaces are converged at the higher T_e for N_m = 2047 whereas only flux surfaces out to r/a ~ 0.5 are converged at the lower T_e.

Figure 4(a) shows the LHRF deposition profile for the higher temperature case at 2047 modes and Fig. 4(b) shows the corresponding electric field contours for the Re {E_ζ} in that case. The power deposition profile is characterized by two peaks. The first corresponds to core absorption at 0 < r/a < 0.3 and is presumably due to the increased central electron temperature which results in stronger core absorption. The second and larger peak at r/a ≈ 0.5 could be interpreted as resulting from waves which are not absorbed completely on the first pass and instead reflect from the plasma edge on the high field side as seen in the electric field contour in Fig. 4(b). Failure of the LH wave front to be absorbed on a single pass into the plasma despite the higher electron temperature is likely due to decreases in the parallel wavenumber arising from the non-constancy of the poloidal mode number in toroidal geometry. After reflection from a cut-off at the plasma edge LH waves then characteristically undergo a large increase in parallel wavenumber (a feature seen in ray tracing calculations) and thus damp strongly off-axis. This would then correspond to the large off-axis peak at r/a ≈ 0.5.

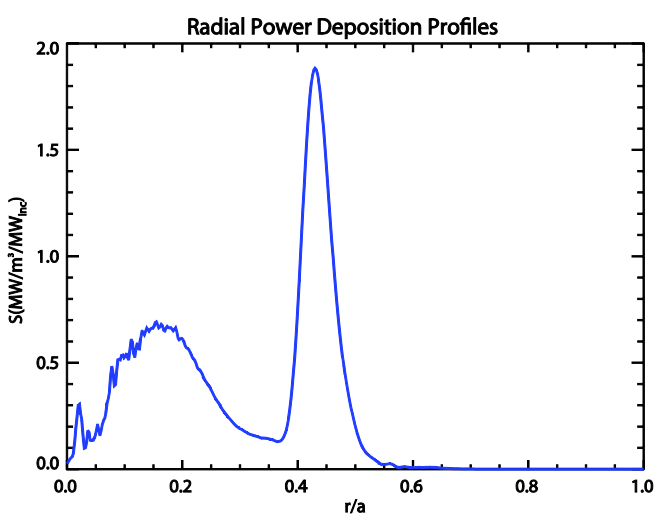

(a)

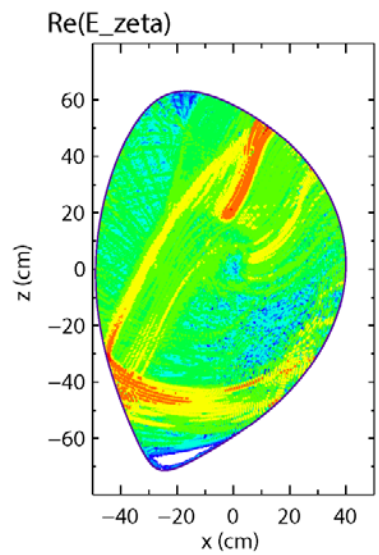

(b)

Figure 4: Results from a TorLH EAST simulation at N_m = 2047 and Te(0) = 9.5 keV. (a) LHRF power deposition to electrons (MW / m^3 / MW incident power) versus r/a. (b) LH electric field contours for the Re{E_ζ}.

Analytic forms of the quasilinear diffusion coefficients for a toroidal geometry that are modified from the Kennel-Engelmann (K-E) diffusion coefficients have been derived [Lee 2018] as discussed in the Summary Section 2(a). The K-E coefficients are based on a homogenous plasma and background magnetic fields along the particle trajectory. This simplification can fail to insure positive-definiteness of the bounce average of the coefficients in toroidal geometry. Our new form guarantees the positive definiteness and includes the toroidal effects more accurately. When the correlation length of plasma-wave interactions is comparable to the length of the magnetic field variation, the variation needs to be considered in the trajectory integral instead of a Dirac-delta function as used in the formulation of the K-E coefficients. For RF waves in a toroidal geometry, the parabolic variation of the magnetic fields in the trajectory integral around the outer-midplane or the inner-midplane is evaluated by Airy functions. This allows the coefficients to include both resonant and non-resonant contributions and capture the correlation between consecutive resonances. Figure 5(b) shows results from the implementation of the new positive definite form of the RF quasilinear diffusion coefficient in TorLH. Velocity space contours of λB are first shown in Fig. 5(a) where λ is the bounce time $\times$ $u_{//0}$ and B is the bounce averaged diagonal component in the speed direction (D_{uu}) of the K-E quasilinear RF diffusion coefficient evaluated using the full-wave fields from a TorLH simulation based on electron Landau damping on a Maxwellian distribution. The white space between contours denotes areas where the diffusion coefficient has become negative. In contrast when the coefficient is evaluated from the new positive definite form using the same TorLH fields [see Fig. 5(b)] it is smooth and continuous and positive everywhere.

Verification of the implementation of the new positive definite form of the K-E diffusion coefficient in TorLH was deferred to the third quarter. This was done by comparing the absorbed power density profile from the new diffusion coefficient formulation in the Fokker Planck solver (CQL3D) with the power deposition from **J·E** simulated with TorLH.

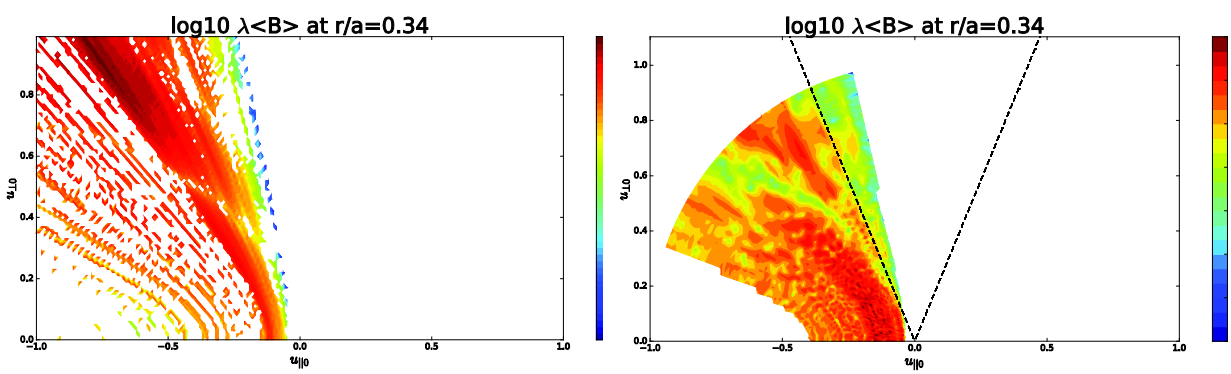

Figure 5: Velocity space contours of λB where λ is the bounce time $\times$ $u_{//0}$ and B is the bounce averaged diagonal component in the speed direction (D_{uu}) of the K-E quasilinear RF diffusion coefficient (cm^5 / s^5) at r/a = 0.34, evaluated using the full-wave fields from a TorLH simulation, based on Maxwellian (linear) electron Landau damping using (a) the standard K-E form and (b) the new positive definite form. Contours are plotted in a ($u_{//0}$, $u_{\perp 0}$) space where u, $u_{//}$, and $u_{\perp}$ are normalized by u_{norm}, which is the electron reference momentum for an energy E_{norm} = 2500 keV. U_{norm} is obtained relativistically from $u_{norm} = [(E_{norm}/m_0c^2+1)^2-1]^{1/2}$=5.8 times the light speed.

3. Completion of the Third Quarter Milestone

Perform iterations between TorLH and CQL3D with moderate poloidal mode resolution (1023 modes) using EAST parameters at high electron temperature for strong electron Landau damping. Determine if an explicit fixed point iteration is needed to achieve a converged solution or if an acceleration method is needed such as a Jacobian-free Newton Krylov technique.

3(a) Summary

During the third quarter we successfully iterated the TorLH full-wave solver and the bounce averaged Fokker Planck solver CQL3D for the EAST discharge parameters employed in the prior quarterly simulations [B_0 = 2.31 T, I_p = 373 kA, a = 0.42 m, R_0 = 1.85 m, $n_e(0) = 3.6 \times 10^{19}$ m^{-3}, n// = -1.8, and f_0 = 4.6 GHz]. The peak electron temperature was varied from 3.2 keV to 16 keV in order to simulate weak and strong electron damping regimes. An explicit fixed point iteration scheme was used with 480 radial elements and 255, 511, and 1023 poloidal modes. Based on simulations with 3-5 iterations between TorLH and CQL3D it was observed that the explicit fixed point iteration scheme worked well in cases of strong wave absorption and that an acceleration method such as the Jacobian-free Newton Krylov technique might be needed in weak damping cases. This finding is consistent with prior experience iterating TorLH and CQL3D for parameters characteristic of Alcator C-Mod LHCD experiments [Wright 2014].

3(b) Details of Third Quarter Progress

The TorLH-CQL3D iteration consists of a complex multi-step workflow that was automated under the Integrated Plasma Simulator (IPS) framework as part of the third quarter milestone. The workflow consists of the following steps:

(i) Execute the TorLH full-wave solver in “solver” mode to obtain the LHRF electric fields assuming the background electron distribution is Maxwellian.

(ii) Execute the TorLH full-wave solver in “qldce” mode to reconstruct the quasilinear RF diffusion coefficient from the LHRF wave fields computed in Step (i).

(iii) Execute the CQL3D Fokker Planck solver to advance the electron distribution function in time using the quasilinear RF diffusion coefficient computed in Step (ii).

(iv) Create a table of interpolating values for $Im\{\chi_{zz}\} \propto \partial f_e / \partial p_{//}$ using the electron distribution function computed by CQLD in Step (c). Here χ_{zz} corresponds to the Stix dielectric tensor element and gives the electron Landau damping physics.

(v) Execute the TorLH full-wave solver in “solver” mode again to obtain the LHRF electric fields this time using the quasilinear electron Landau damping evaluated in Step (iv).

(vi) Repeat Steps (ii)-(v) until convergence is achieved between the electron distribution function and the RF wave fields.

Before iterating further at high LHRF power ($\geq$ 2 MW) it was decided to carry out a detailed verification exercise whereby the LH power was reduced to 1 W. In this case, as the codes are iterated, the final converged electron distribution function should remain Maxwellian since at very low RF power there is no distortion or "plateau" formation in the electron distribution function. The resulting power absorption profiles in TorLH and CQL3D should be identical and the integrated RF powers in TorLH and CQL3D should also be the same (in this case 1 W). This verification exercise was deferred to the fourth quarter where it was completed.

4. Completion of the Fourth Quarter Milestone

Perform iterations between TorLH and CQL3D at high poloidal mode resolution (4095 modes). Use EAST parameters with strong electron damping and then with weak electron damping. Compare converged results for power deposition and hard x-ray emission with ray tracing / Fokker Planck predictions from GENRAY / CQL3D.

4(a) Summary

In order to complete the third quarter milestone the LH power was increased to ~ 1MW using an exponential turn-on function that was implemented using the IPS workflow. It was decided to use this type of turn-on in order to eliminate oscillatory behavior in the explicit fixed point iteration scheme described by steps (i) – (vi) in Section 3(b), thus achieving a quasilinear diffusion coefficient consistent with the local electron distribution function. The form of exponential turn-on of the LH power was given by:

$$P_{LH}(i) = P_{Floor} \text{ for } i = 0, \qquad 3(a)$$

$$P_{LH} = P_{LH0}\left[1 - \exp[-(i - i_0)/p_{on}]\right] \text{ for } i \geq 1, \qquad 3(b)$$

where P_{Floor} = 10W corresponding to Maxwellian damping, P_{LH0} is the final target LH power, i refers to the iteration number between TorLH and CQL3d, $i_0 = 0$ to start the iteration from a Maxwellian, and p_{on} is the turn-on rate which in this case was set to $p_{on} = 5$. This type of LH power turn-on resulted in an iteration scheme that was remarkably stable, thus eliminating the need to implement an acceleration method such as the Jacobian-free Newton Krylov technique.

4(b) Details of Fourth Quarter Progress

The third quarter milestone had explicitly called to:

> *Perform iterations between TorLH and CQL3D with moderate poloidal mode resolution (1023 modes) using EAST parameters at high electron temperature for strong electron Landau damping. Determine if an explicit fixed point iteration is needed to achieve a converged solution or if an acceleration method is needed such as a Jacobian-free Newton Krylov technique.*

This was then completed during the fourth quarter using EAST discharge parameters employed in the prior quarterly simulations [B_0 = 2.31 T, I_p = 373 kA, a = 0.42 m, R_0 = 1.85 m, $n_e(0) = 3.6 \times 10^{19}$ m^{-3}, $T_e(0)$ = 3.2 keV, f_0 = 4.6 GHz, and P_{LH} ~ 1MW]. An important variation on the prior quarterly milestones that was done in the fourth quarter was to simulate the strong electron damping case by using high parallel refractive index ($n_{//}$ ~ 5.5), rather than increasing the background electron temperature to ~ 16keV. This provides for a more consistent comparison of the strong electron Landau damping case with the case of weak damping ($n_{//}$ ~ 1.8), because the MHD equilibria remain the same since the plasma β is unchanged. The results at the tenth

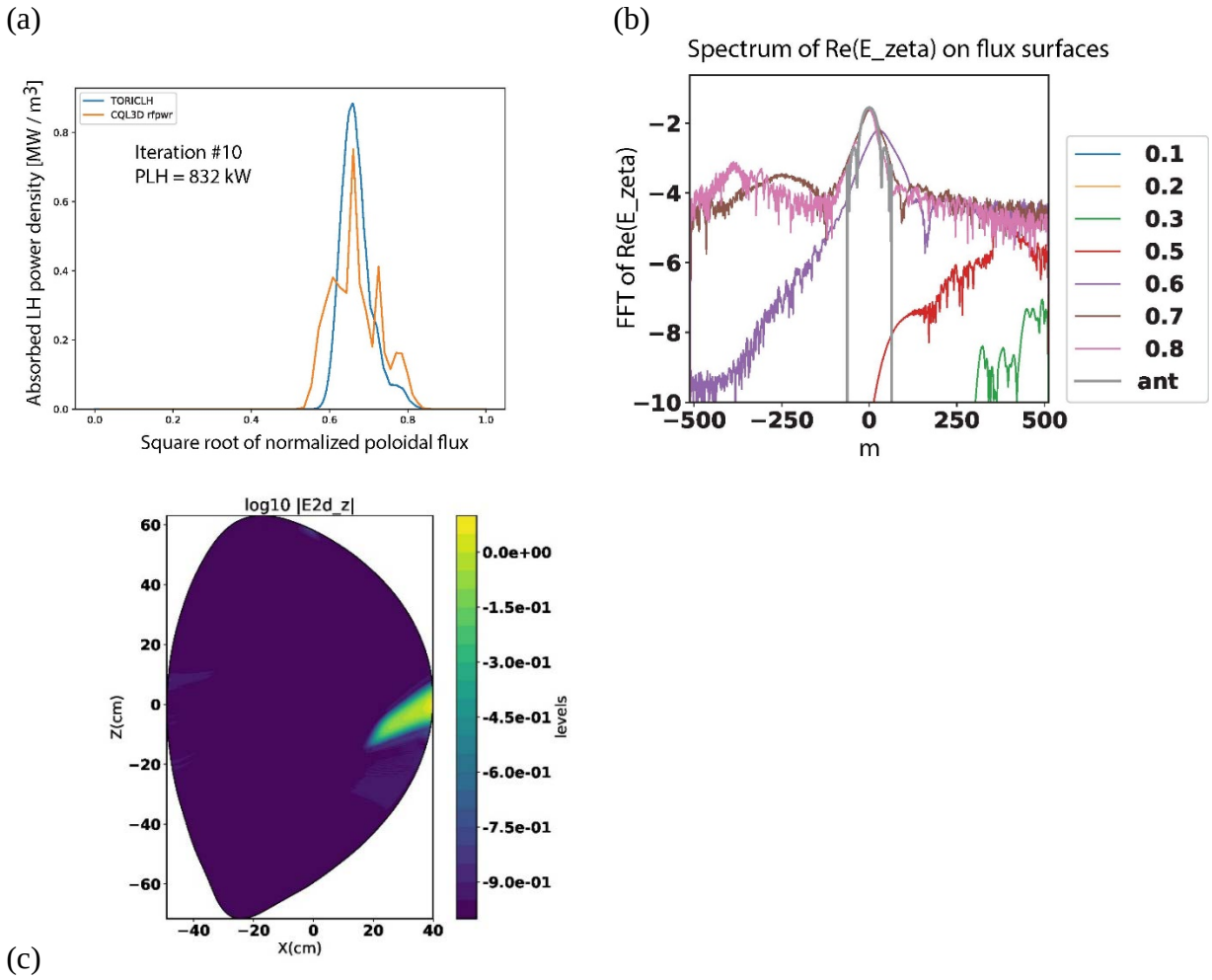

Figure 6: Coupled TorLH-CQL3D simulation of LH wave propagation and quasilinear damping in the EAST tokamak using 480 radial elements, 1023 poloidal modes, $n_{//}$ = -5.5 with [B_0 = 2.31 T, I_p = 373 kA, a = 0.42 m, R_0 = 1.85 m, $n_e(0) = 3.6 \times 10^{19}$ m^{-3}, $T_e(0)$ = 3.2 keV, f_0 = 4.6 GHz, and P_{LH0} = 1MW]. Results shown for iteration #10. (a) Comparison of LHRF power deposition profiles from TorLH (blue curve) and CQL3D (tan color curve) versus square root of normalized poloidal flux. (b) FFT of the $Re(E_\zeta)$ electric field component (Log_{10} scale) versus poloidal mode number m on selected flux surfaces. Flux surface labels correspond to square root of normalized poloidal flux. (c) 2-D contours of the $|Re(E_\zeta)|$ electric field component (Log_{10} scale).

iteration between between TorLH and CQL3D are shown in Figs. 6(a)-(c). The deposition profiles from TorLH and CQL3D agree qualitatively in shape at the tenth iteration where the LH power is 832 kW. Iterating further brings the profile shapes into quantitative agreement as will be shown later for the weak absorption case. Although the flux surfaces appear to be fully converged at all radii in Fig. 6(b), it was found that as the number of poloidal modes is increased to 2047 the FFT of the electric field on the outer flux surfaces (r/a > 0.7) starts to rise, with full convergence not achieved until 4095 modes. The larger number of poloidal modes needed for actual convergence is expected from prior analysis and simulation since $n_{//}$ = 5.5 corresponds to a perpendicular wave number of $k_\perp \sim 46$ cm^{-1}. In order to resolve the shortest wavelength in the

system we set $k_\perp \sim (m/r)$ to get m ~ 2070 at r ~ 45cm, and $N_m \sim 2m + 1 \sim 4140$. The contour plot for the $|Re(E_\zeta)|$ in Fig. 6(c) clearly shows the strong single pass damping in this case.

Thus implementation of the exponential turn-on of the LH power in the TorLH-CQL3D fixed point iteration scheme and the iteration to convergence of a TorLH-CQL3D simulation with strong electron damping using ~ 1023 poloidal modes substantially satisfies the language of the third quarter milestone stated above.

The fourth quarter milestone proposed in order to accomplish the 2017 Theory Performance Target was:

> *Perform iterations between TorLH and CQL3D at high poloidal mode resolution (4095 modes). Use EAST parameters with strong electron damping and then with weak electron damping. Compare converged results for power deposition and hard x-ray emission with ray tracing / Fokker Planck predictions from GENRAY / CQL3D.*

One of the challenges encountered performing multiple high resolution TorLH simulations as part of the TorLH-CQL3D iteration was that we started to sample the failure rate of nodes on Edison. The 4095 poloidal mode simulations using 480 radial elements required 32,640 cores. However only half of the 24 available cores on each node could be used because of memory per node limits, necessitating a reservation of 2720 nodes with a total charged core count of 65,280, which is about half of the available cores on Edison. Simulations requiring ~ 10-12 hours of wall clock time encountered hardware failures in the form of node interconnect errors every 4-6 hours. A restart capability had been implemented in the IPS during prior work which allowed us to restart the TorLH-CQL3D iteration sequence from the prior iterate each time a hardware error was encountered. However, each time an error occurred it would cost about 200,000 MPP hours. Consequently, we were only able to perform 2 iterations at 4095 modes for the strong absorption case with $n_{//} = -5.5$ and 5 iterations at 4095 modes for the weak absorption case with $n_{//} = -1.8$. More sophisticated methods for mitigating these types of errors are currently being implemented in order to reliably run TorLH for 10-20 iterations.

In Fig. 7 we present simulation results for the strong absorption case with $n_{//} = -5.5$, 4095 poloidal modes, and 480 radial elements. Because of hardware errors discussed above the simulation only advanced to the second iteration where the LH power was ~ 180 kW. Because of the low power, the distribution function is not far from Maxwellian and the power deposition profiles from TorLH and CQL3D are still close to each other [see Fig. 7(a)]. Figure 7(b) shows that the electric fields are converged on nearly all flux surfaces as expected from analytic estimates using 4095 poloidal modes. Convergence at r/a > 0.8 is somewhat marginal in this case although iterating to higher LH power could change that result.

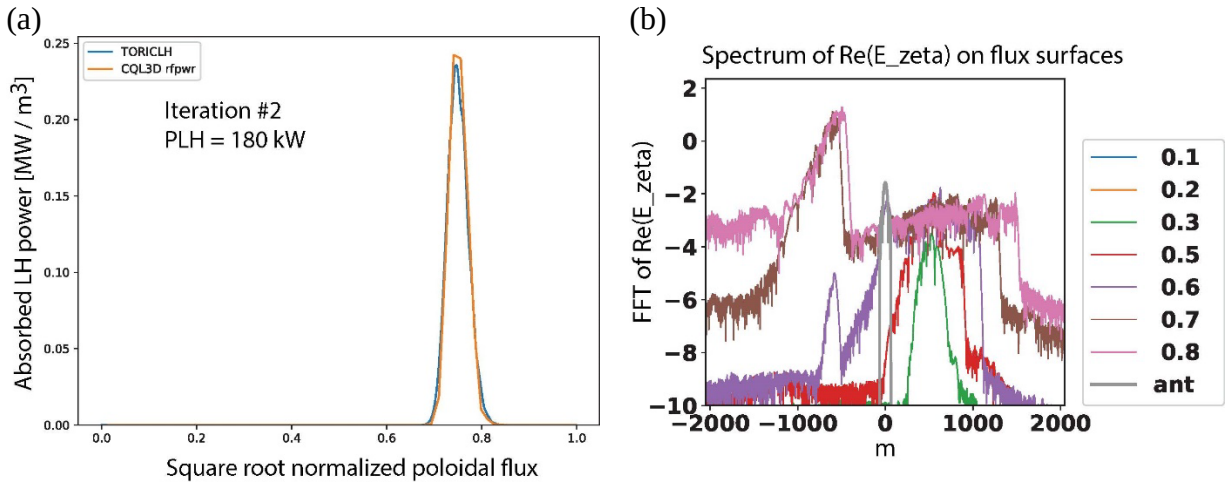

Figure 7: Coupled TorlH-CQL3D simulation of LH wave propagation and quasilinear damping in the EAST tokamak using 480 radial elements, 4095 poloidal modes, $n_{//}$ = -5.5 with [B_0 = 2.31 T, I_p = 373 kA, a = 0.42 m, R_0 = 1.85 m, $n_e(0) = 3.6 \times 10^{19}$ m^{-3}, $T_e(0)$ = 3.2 keV, f_0 = 4.6 GHz, and P_{LH0} = 1MW]. (a) Comparison of LHRF power deposition profiles from TorLH (blue curve) and CQL3D (tan color curve) versus square root of normalized poloidal flux. (b) FFT of the Re(E_ζ) electric field component (Log_{10} scale) versus poloidal mode number m on selected flux surfaces. Flux surface labels correspond to square root of normalized poloidal flux.

We have also simulated the weak absorption case with 4095 poloidal modes, 480 radial elements, and $n_{//}$ = -1.8. The results shown in Figs. 8(a)-8(c) correspond to the fifth iteration between TorLH and CQL3D, which was achieved with one restart after a hardware failure on an earlier iteration. As shown in Fig. 8(a), the LH power at iteration 5 is ~ 531 kW, which results in significant distortion of the electron distribution function which manifests itself as disagreement early on between the CQL3D and TorLH power deposition profiles. Figure 8(b) indicates the electric field solutions are clearly converged at 4095 modes. The asymmetry of the electric field distribution with respect to poloidal mode number on each flux occurs because the fields are determined by electron Landau damping for negative m and LH wave accessibility for positive m. Note that for EAST the toroidal mode number is negative so that negative m increases $k_{//}$ and positive m decreases $k_{//}$. The corresponding 2-D contours of electric field in Fig. 8(c) show a concentration of wave fields on the high field side of the tokamak where wave accessibility is better and characteristic reflections of the wave fields from the top edge of the tokamak, which is seen in cases of weak absorption.

The lack of convergence between the CQL3D and TorLH deposition profiles shown in Fig. 8(a) is normal for early in this type of explicit fixed point iteration scheme with weak electron Landau damping. Figures 9(a) – 9(c) demonstrate the remarkable level of agreement that can be expected between the CQL3D and TorLH power deposition profiles with subsequent iterations between CQL3D and TorLH. Shown are the power deposition profiles for the fifth, tenth, and fifteenth iterates using 480 radial elements, 1023 poloidal modes, and $n_{//}$ = -1.8 with the same EAST plasma parameters as in Fig. 8. This case iterates without failure since the number of cores needed in the simulation is relatively modest at ~2200. An attractive feature of the results

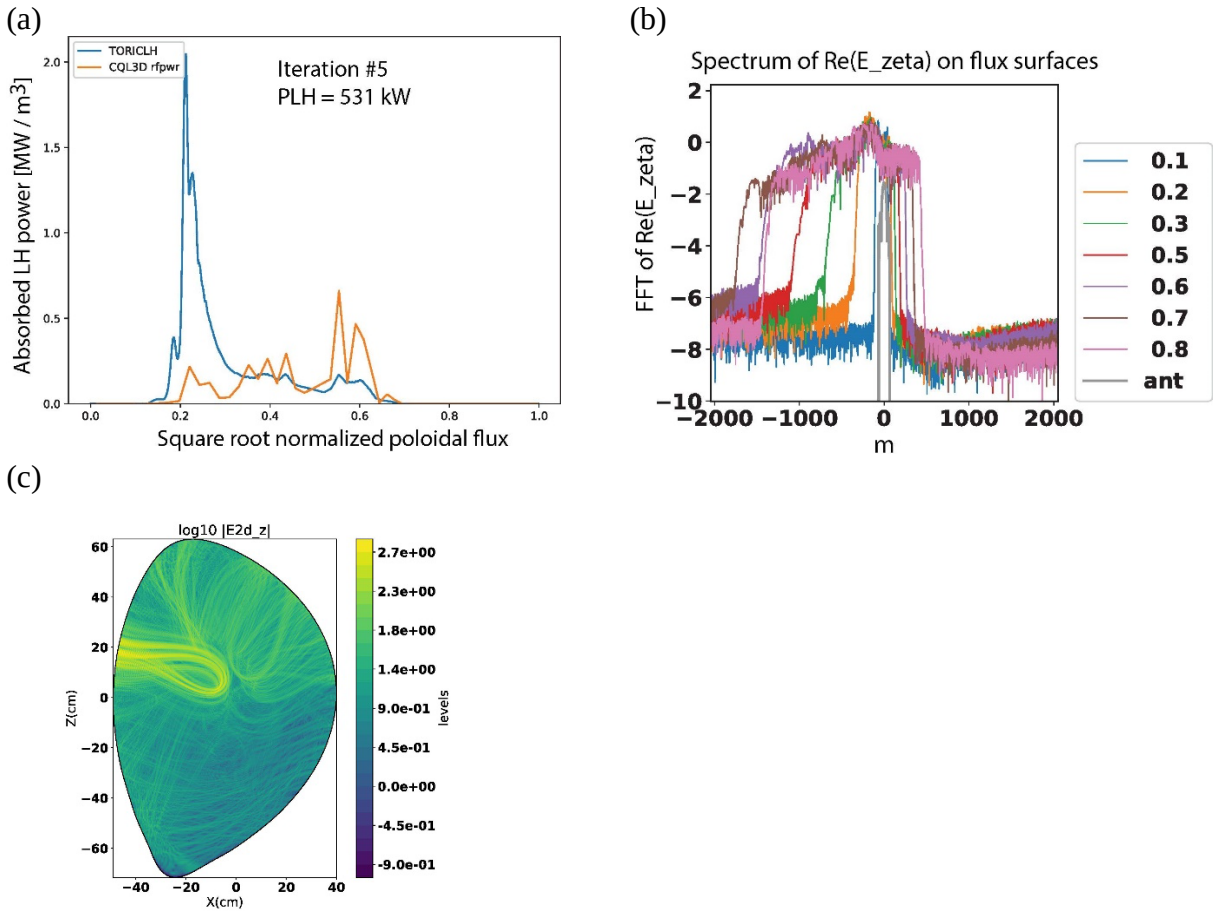

Figure 8: Coupled TorLH-CQL3D simulation of LH wave propagation and quasilinear damping in the EAST tokamak using 480 radial elements, 4095 poloidal modes, $n_{//}$ = -1.8 with [B_0 = 2.31 T, I_p = 373 kA, a = 0.42 m, R_0 = 1.85 m, $n_e(0) = 3.6 \times 10^{19}$ m^{-3}, $T_e(0)$ = 3.2 keV, f_0 = 4.6 GHz, and P_{LH0} = 1MW]. Results shown for iteration #5. (a) Comparison of LHRF power deposition profiles from TorLH (blue curve) and CQL3D (tan color curve) versus square root of normalized poloidal flux. b) FFT of the $Re(E_\zeta)$ electric field component (Log_{10} scale) versus poloidal mode number m on selected flux surfaces. Flux surface labels correspond to square root of normalized poloidal flux. (c) 2-D contours of the $|Re(E_\zeta)|$ electric field component (Log_{10} scale).

in Fig. 9 is that there is an orderly progression towards converged power deposition profiles as the LH power is turned on and TorLH and CQL3D are iterated. This is in contrast to situations where the deposition profiles oscillate between two solutions from one iterate to the next. Exponential turn-on of the LH power is thought to be critical in order to eliminate this unwanted oscillatory behavior.

The final part of the fourth quarter milestone called for a comparison of the converged results for power deposition and hard x-ray emission with ray tracing / Fokker Planck predictions [Shiraiwa 2015] from GENRAY / CQL3D for these same EAST discharge parameters. The final iterated profiles from TorLH-CQL3D have not yet been achieved at the highest poloidal mode resolution. However, the preliminary results shown in Fig. 8 for $n_{//}$ = -1.8 at 4095 modes and the converged results shown in Fig. 9 for $n_{//}$ = -1.8 at 1023 modes indicate the profiles of LHRF power absorption and hard x-ray emission will be substantially off-axis, which agrees with the ray

tracing / Fokker Planck simulation results, but disagrees with experiment where the measured hard x-ray profiles in EAST tended to be more peaked on-axis (see Fig. 4 of [Shiraiwa 2015]).

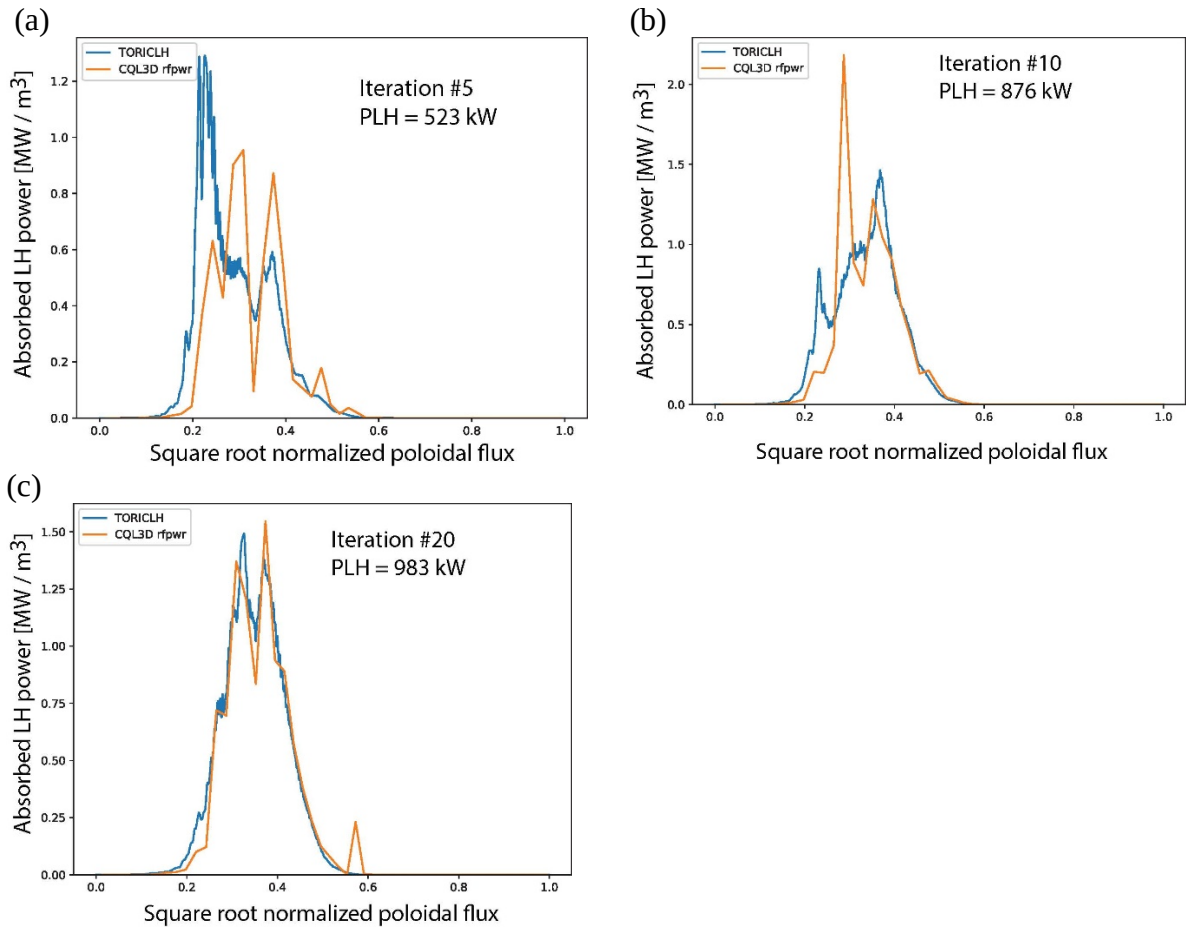

Figure 9: Coupled TorLH-CQL3D simulation of LH wave propagation and quasilinear damping in the EAST tokamak using 480 radial elements, 1023 poloidal modes, $n_{//} = 1.8$ with [$B_0 = 2.31$ T, $I_p = 373$ kA, a = 0.42 m, $R_0 = 1.85$ m, $n_e(0) = 3.6 \times 10^{19}$ m^{-3}, $T_e(0) = 3.2$ keV, $f_0 = 4.6$ GHz, and $P_{LH0} = 1$MW]. Comparison of LHRF power deposition profiles from TorLH (blue curve) and CQL3D (tan color curve) versus square root of normalized poloidal flux at (a) the fifth iteration, (b) the tenth iteration, and (c) the twentieth iteration.

References

[Batchelor 2009] D. Batchelor, G. Abla, E. D'Azevedo, G. Bateman, D. E. Bernholdt, L. Berry, P. Bonoli, R. Bramley, J. Breslau, M. Chance, J. Chen, M. Choi, W. Elwasif, S. Foley, G. Fu, R. Harvey, E. Jaeger, S. Jardin, T. Jenkins, D. Keyes, S. Klasky, S. Kruger, L. Ku, V. Lynch, D. McCune, J. Ramos, D. Schissel, D. Schnack and J. Wright, "Advances in simulation of wave interactions with extended MHD phenomena", Journal of Physics: Conference Series **180**, 012054 (2009).

[Bonoli 2014] P. T. Bonoli, “Review of recent experimental and modeling progress in the lower hybrid range of frequencies at ITER relevant parameters”, Physics of Plasmas **21**, 061508 (2014).

[Harvey 1992] R.W. Harvey and M.G. McCoy, "The CQL3D Fokker-Planck Code", GA Report GA-A20978. Published in Proc. of IAEA Technical Committee Meeting on Advances in Simulation and Modeling of Thermonuclear Plasmas, Montreal, 1992, p. 527, IAEA, Vienna (1993).

[Kennel & Engelmann 1966] C. F. Kennel and F. Engelmann, “Velocity Space Diffusion from Weak Plasma Turbulence in a Magnetic Field”, Physics of Fluids **9**, 2377 (1966).

[Lee 2018] J. P. Lee, D. Smithe, J. C. Wright and P. T. Bonoli, “A positive-definite form of bounce- averaged quasilinear velocity diffusion for the parallel inhomogeneity in a tokamak”, Plasma Physics and Controlled Fusion **60**, 025007 (2018).

[Shiraiwa 2015] S. Shiraiwa, S. G. Baek, I. Faust, G. Wallace, P. Bonoli, O. Meneghini, R. Mumgaard, R. Parker, S. Scott, R. W. Harvey, B. J. Ding, M. H. Li, S. Y. Lin, and C. Yang, “Impact of SOL plasma profiles on lower hybrid current drive: Experimental evidence, mitigation and modeling approaches”, AIP Conference Proceedings **1689**, 030016 (2015).

[Wright 2009] J. C. Wright, P.T. Bonoli, A. E. Schmidt, C. K. Phillips, E. Valeo, R. W. Harvey, and M. Brambilla, “An assessment of full wave effects on the propagation and absorption of lower hybrid waves,” Phys. Plasmas **16**, 072502 (2009).

[Wright 2014] J. C. Wright, A. Bader, L. A. Berry, P. T. Bonoli, R. W. Harvey, E. F. Jaeger, J.-P. Lee, A. Schmidt, E. D’Azevedo, and I. Faust, “Time dependent evolution of RF-generated non-thermal particle distributions in fusion plasmas”, Plasma Physics and Controlled Fusion **56**, 045007 (2014).